SCEC Award Number 25202

Spatiotemporal interpolation and correction of perturbations in GNSS time series and velocity products for the Community Geodetic Model

Final Report

Michael Floyd, Thomas Herring

Massachusetts Institute of Technology

Statewide Combination of GNSS Velocities for the Community Geodetic Model

We have produced a comprehensive GNSS velocity solution over all of California and western Nevada for the Community Geodetic Model (CGM). We download, realign and combine publicly available velocity products from six sources (four continuous GNSS only, one survey GNSS only and one continuous and survey GNSS). This is an extension of the work reported in SCEC Award Number 24065.

We download and use the fundamental no-net-rotation (NNR) reference frame versions of various analysis centers' velocity products (IGS20 for NGL/UNR, and ITRF2014 for GAGE/CWU, JPL and SOPAC) except for the USGS velocity solution for which we use the North America reference frame version due to its consistent alignment versus a transition, and therefore discontinuity, introduced in the processing on June 1, 2024 (Jessica Murray, USGS, pers. comm.) for the NNR solution. Sources and URLs are summarized in Table 1. The NGS NCN "MYCS3" solution (in ITRF2020) provides velocities but no associated uncertainties (to inform weighting in our combination), so we downweight this solution at this time, by assigning velocity sigmas of 9999.99 mm/yr, so as to be effectively not included. We rotate the USGS solution from North America defined by Altamimi et al.'s (2017) ITRF2014 plate motion model to an NNR reference frame (Jessica Murray, USGS, pers. comm.). As expected, the USGS North America-rotated-to-NNR is slightly different to its published NNR (ITRF2014) solution due to the processing transition (weighted root-mean-square difference is 0.12 mm/yr in the east component, 0.16 mm/yr in north and 0.23 mm/yr in up). Other solutions where two reference frames are available (GAGE/CWU and NGL/UNR) match exactly if one is transformed to the other using the documented plate rotation rate vector (Altamimi et al., 2017, for the former and Kreemer et al., 2014, for the latter). No origin rate bias (translation rate) is considered during these transformations (e.g. Altamimi et al., 2023).

For the NGL/UNR solution, the NNR solution file is also the only one to contain all sites, whereas their velocity files referenced to tectonic plates (Kreemer et al., 2018) contain only sites on each tectonic plate (as defined by Bird's, 2003, plate boundaries), so we prefer to start with

this global file and transform it accordingly. There are negligible rate differences, on the order of 0.1 mm/yr along the Y and Z axes of the geocentric, Earth centered-Earth fixed coordinates system (e.g. https://itrf.ign.fr/en/solutions/transformations), between the fundamental no-net-rotation reference frames of ITRF2020 versus ITRF2014 (the basis for IGS14 and IGb14) and ITRF2008 (the basis of IGS08 and IGb08). So we do not first apply any realignments of each velocity solution relative to any of the others, although we could estimate and apply such additional transformations.

We combine the velocity solutions by calculating, for each station *j*, the weighted mean, $\bar{v}_j$, using the inverse variances, $1/\sigma_i^2$, of the station velocity quoted in each analysis center *i*'s product as the weight (Equation 1). We test definitions of the associated uncertainties in three ways: using the inverse of the sum of the weights, which is equivalent to the formal uncertainties from weighted least-squares inversions (Equation 2); using the standard weighted unbiased sample standard deviation (Equation 3); and using the variance sum of these two (Equation 4).

$$\bar{v}_j = \sum_{i=1}^{n} \frac{v_i}{\sigma_i^2} \Big/ \sum_{i=1}^{n} \frac{1}{\sigma_i^2} \tag{1}$$

$$\bar{\sigma}_j = \sqrt{1 \Big/ \sum_{i=1}^{n} \frac{1}{\sigma_i^2}} \tag{2}$$

$$\bar{s}_j = \sqrt{\frac{\sum_{i=1}^{n} \frac{\left(v_i - \bar{v}_j\right)}{\sigma_i^2}}{\sum_{i=1}^{n} \frac{1}{\sigma_i^2} - \sum_{i=1}^{n} \left(\frac{1}{\sigma_i^2}\right)^2 \Big/ \sum_{i=1}^{n} \frac{1}{\sigma_i^2}}} \tag{3}$$

$$\bar{s}_j = \sqrt{1 \Big/ \sum_{i=1}^{n} \frac{1}{\sigma_i^2} + \frac{\sum_{i=1}^{n} \frac{\left(v_i - \bar{v}_j\right)}{\sigma_i^2}}{\sum_{i=1}^{n} \frac{1}{\sigma_i^2} - \sum_{i=1}^{n} \left(\frac{1}{\sigma_i^2}\right)^2 \Big/ \sum_{i=1}^{n} \frac{1}{\sigma_i^2}}} \tag{4}$$

The inverse of the sum of the weights (Equation 2) is only dependent on the velocity sigmas, which can be very small (~ 0.1 mm/yr) for long-running continuous GNSS sites, which make up the vast majority of the networks and their solutions in the western U.S., and is such a small number when taken over a number of contributing solutions that it is largely unrealistic and contributes little to the sum in Equation 4 (first term on the right side). Both definitions of uncertainty in Equations 3 and 4 are therefore nearly identical in this case. The weighted

unbiased sample standard deviation is not only dependent on inverse variance weighting of each solution but also the differences between them (or at least between each and the weighted mean value). It is therefore our preferred definition because it incorporates some level of both

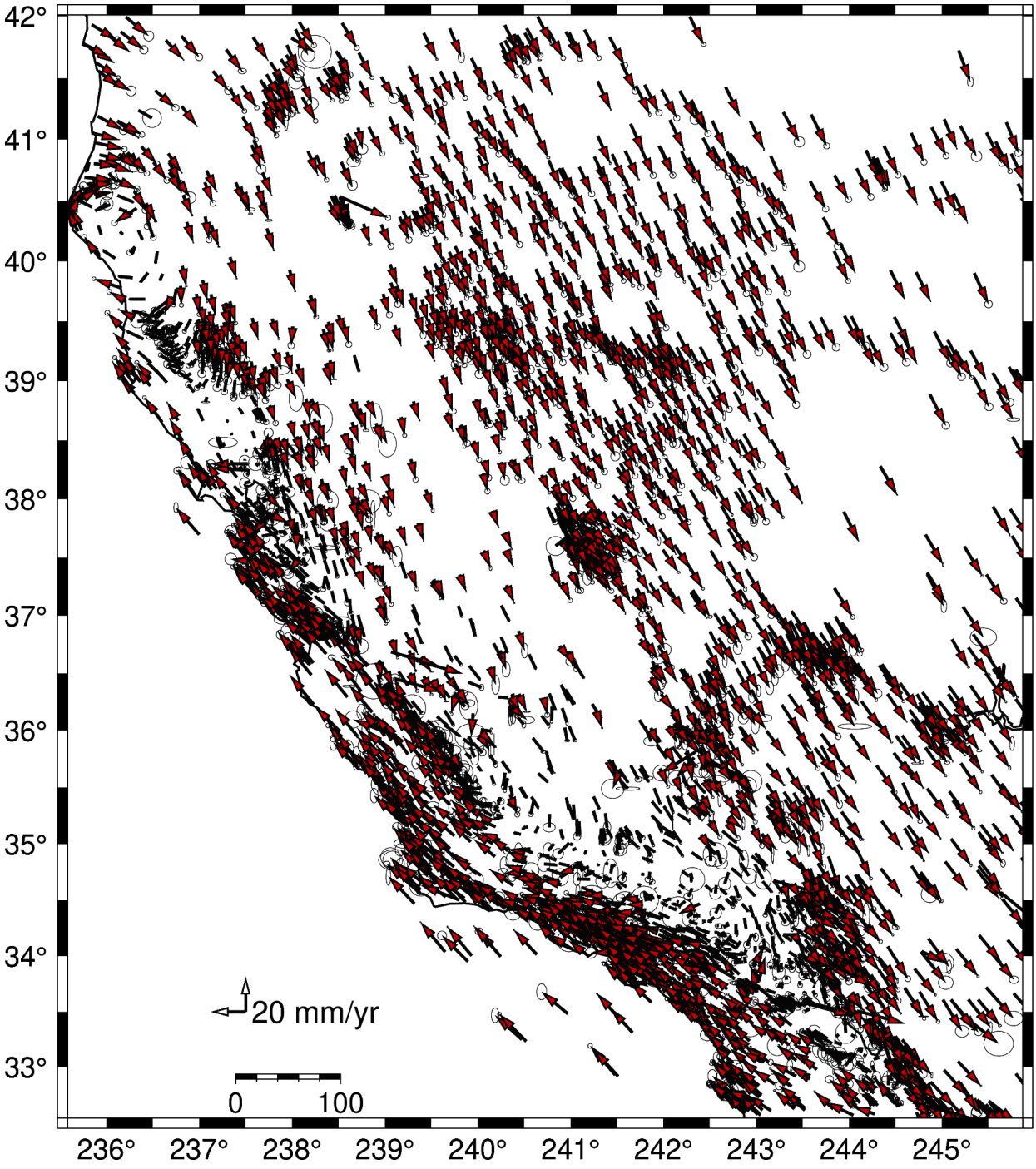

Figure 1: New GNSS velocity solution, rigorously combining continuous and survey GNSS velocities from various analysis centers' publicly available products, as described in this report, for California and western Nevada relative to a North America and Pacific "half-plate" reference frame.

aleatoric uncertainty (from the precision of the velocities quoted by the various analysis centers' methods) and some level of epistemic uncertainty (from the variation of results produced by different means from the same data).

We bound the solution to California (and western Nevada) within the region of 124.417°W to 114.133°W and 32.534°N to 42.010°N, as shown in Figure 1. Finally, we rotate the GNSS velocities into various common reference frames used to describe and study the North America-Pacific plate boundary. We produce velocities relative to North America and the Pacific plate defined by Altamimi et al. (2023) for the ITRF2020 plate motion model, Altamimi et al. (2017) for the ITRF2014 plate motion model, Kreemer et al. (2014) for the Global Strain Rate Model, and Kreemer et al. (2018) for an updated definition of North America only. We also produce velocities in "half-plate" reference frames, by taking the average rotation rate vectors of the North America-Pacific plate pairs where simultaneously defined by the publications cited above, which minimizes the velocities along the plate boundary itself rather than in the far-field on either side (Figure 1).

Ultimately, this approach is very similar to that of Zeng (2022) for the 2023 National Seismic Hazard Model, in both analysis center sources and combination approach. Compared to their compilation, within the same region defined above and for velocities with sigmas less than or equal to 4.143 mm/yr in both horizontal components, the largest for any site within the region of interest from the Zeng (2022) solution, we present about 3320 sites, 450 more than the 2870 from the Zeng (2022) solution within the same criteria.

Spatial Interpolation by Colocation

A fundamental goal of the CGM is to produce continuous fields of surface displacement rate and strain rate for the study of crustal deformation. We use the combined velocity solution described above as input to colocation to produce an updated strain rate field for California and western Nevada (Figure 2).

Colocation calculates an empirical spatial covariance matrix, $\mathbf{C}_{xx}$, from the data, x, to interpolate between data locations, e.g.

$$\widehat{y} = C_{yx} C_{xx}^{-1} x \tag{5}$$

The gradient of the resulting interpolated velocity field can be separated into components including the shear strain rate, which is most meaningful for the strike-slip faults throughout California.

The primary details of the derived strain rate field are familiar from many previous studies but the method and fundamental velocity solution presented here are an improvement over previous work and one contribution to the CGM (the velocity solution to the GNSS

component of CGM products and the colocation method as one among many approaches to interpolate the geodetic data to produce velocity and strain rate fields for comparison).

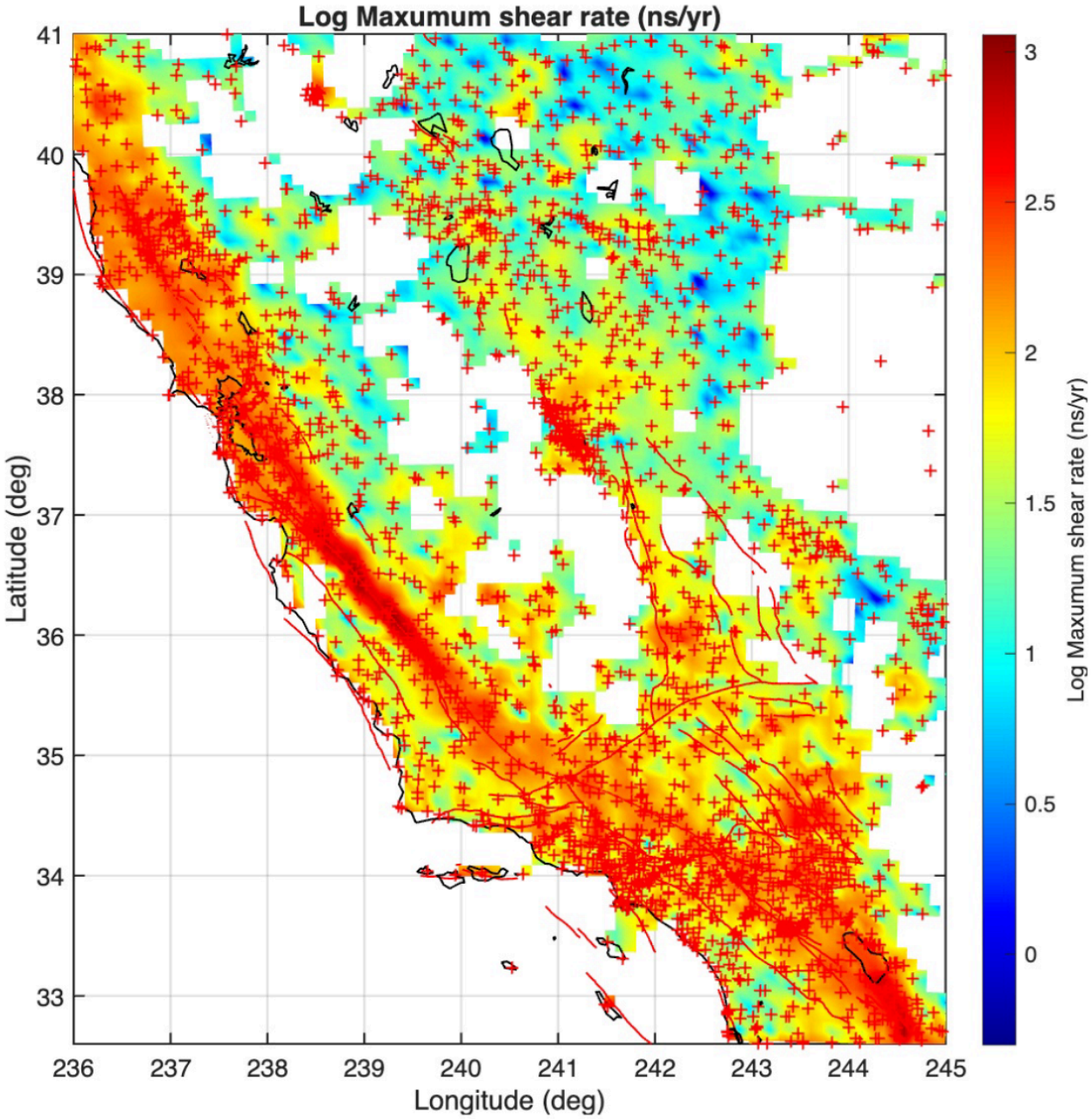

Figure 2: Spatially interpolated strain rate by colocation of the velocity solution shown in Figure 1.

Product	Analysis Center	URL(s)	Reference(s)
GAGE	Central Washington University (CWU); Massachusetts Institute of Technology (MIT)	https://data.earthscope.org/archive/gnss/products/velocity/	Herring et al. (2016)
ESESES MEaSUREs	JPL	https://cddis.nasa.gov/archive/GPS_Explorer/archive/velocities/ https://garner.ucsd.edu/pub/measuresESESES_products/Velocities/	Bock et al. (2023)
	SOPAC		
	Combination [not used]		
NOAA CORS Network (NCN)	National Geodetic Survey (NGS)	https://geodesy.noaa.gov/corsdata/coord/coord_20/	
Nevada Geodetic Laboratory (NGL)	University of Nevada, Reno (UNR)	https://geodesy.unr.edu/gps_timeseries/IGS20/	Blewitt et al. (2018)
USGS	USGS	https://earthquake.usgs.gov/monitoring/gps	Murray and Svarc (2017)
Southern California Earthquake Center survey GPS	Z.-K. Shen	http://scec.ess.ucla.edu/~zshen/cgm/	Shen et al. (2011); Shen (2020); and further updates

Table 1: Summary of the sources used for our combination of velocities across California and western Nevada.

References

Altamimi, Z., Métivier, L., Rebischung, P., Rouby, H., & Collilieux, X. (2017). ITRF2014 plate motion model, *Geophys. J. Int.*, 209 (3), 1906–1912. https://doi.org/10.1093/gji/ggx136.

Altamimi, Z., Métivier, L., Rebischung, P., Collilieux, X., Chanard, K., & Barnéoud, J. (2023). ITRF2020 plate motion model. *Geophys. Res. Lett.*, 50, e2023GL106373. https://doi.org/10.1029/2023GL106373.

Bird, P. (2003). An updated digital model of plate boundaries. *Geochem. Geophys. Geosyst.*, 4, 1027, doi:10.1029/2001GC000252, 3.

Blewitt, G., Hammond, W. C., & Kreemer, C. (2018). Harnessing the GPS data explosion for interdisciplinary science, *Eos*, 99. https://doi.org/10.1029/2018EO104623

Bock, Y., Fang, P., Knox, A., Sullivan, A., Jiang, S., Guns, K., Golriz, D., Moore, A., Argus, D., Liu, Z., & Kedar, S. (2023). Extended Solid Earth Science ESDR System (ES3): Algorithm Theoretical Basis Document (ATBD). http://sopac-csrc.ucsd.edu/index.php/measures-2/

Herring, T. A., Melbourne, T. I., Murray, M. H., Floyd, M. A., Szeliga, W. M., King, R. W., Phillips, D. A., Puskas, C. M., Santillan, M., & Wang, L. (2016). Plate Boundary Observatory and related networks: GPS data analysis methods and geodetic products, *Rev. Geophys.*, 54, 759–808. https://doi.org/10.1002/2016RG000529

Kreemer, C., G. Blewitt, & E. C. Klein (2014). A geodetic plate motion and Global Strain Rate Model, *Geochem. Geophys. Geosyst.*, 15, 3849–3889, doi:10.1002/2014GC005407.

Kreemer, C., Hammond, W. C., & Blewitt, G. (2018). A robust estimation of the 3-D intraplate deformation of the North American plate from GPS. *J. Geophy. Res. Solid Earth*, 123, 4388–4412. https://doi.org/10.1029/2017JB015257

Murray, J. R., & Svarc, J. (2017). Global Positioning System Data Collection, Processing, and Analysis Conducted by the U.S. Geological Survey Earthquake Hazards Program. *Seismol. Res. Lett.*, 88 (3), 916–925. https://doi.org/10.1785/0220160204

Shen, Z.-K. (2020). Updating Campaign GPS Time Series for Integrated Community Geodetic Model. Project Report for SCEC Award 20182. https://central.scec.org/proposal/report/20182

Shen, Z.-K., King, R. W., Agnew, D. C., Wang, M., Herring, T. A., Dong, D., & Fang, P. (2011). A unified analysis of crustal motion in Southern California, 1970–2004: The SCEC crustal motion map, *J. Geophys. Res.*, 116, B11402, https://doi.org/10.1029/2011JB008549

Zeng, Y. (2022). GPS Velocity Field of the Western United States for the 2023 National Seismic Hazard Model Update. *Seismol. Res. Lett.*, 93 (6), 3121–3134, doi:10.1785/0220220180